

TEXTURE SYNTHESIS GUIDED BY A LOW-RESOLUTION IMAGE

M. El Gheche^{1,2}, *J.-F. Aujol*¹, *Y. Berthoumieu*², *C.-A. Deledalle*¹, *R. Fablet*³

¹IMB and ²IMS CNRS laboratories,
IPB, Université de Bordeaux, Talence, France
{mireille.el-gheche, yannick.berthoumieu}@u-bordeaux.fr
{jean-francois.ujol, charles-alban.deledalle}@math.u-bordeaux1.fr

³Institut Mines-Télécom,
Télécom Bretagne; UMR 6285 LabSTICC
Technopôle Brest Iroise, Brest, France
ronan.fablet@telecom-bretagne.eu

ABSTRACT

In this paper, we aim at synthesizing a texture from a high-resolution patch and a low-resolution image. To do so, we solve a nonconvex optimization problem that involves a statistical prior and a Fourier spectrum constraint. The numerical analysis shows that the proposed approach achieves better results (in terms of visual quality) than state-of-the-art methods tailored to super-resolution or texture synthesis.

Index Terms— Texture synthesis, Super resolution, Wasserstein distance, Random phase texture, Proximal algorithms, Nonconvex optimization.

1. INTRODUCTION

Texture synthesis consists of creating a large, coherent, and non-periodic texture image from a given sample. In this paper, we deal with the problem of texture synthesis under the assumption that a low-resolution version of the sought texture is available in addition of the given high-resolution sample. Roughly speaking, based on the down-sampling factor r , the following two cases may occur:

- If r is low, the resulting problem is similar to image reconstruction, with the addition of a high-resolution patch.
- If r is high, the resulting problem is similar to texture synthesis, with the addition of a low-resolution image.

The present paper is placed in the second context.

1.1. Related work

The problem addressed in this paper is closely related to texture synthesis. In fact, when no low-resolution is available, the two problems are identical. Existing texture synthesis algorithms can be broadly categorized into region-growing local methods and optimization-based global methods. Local approaches grow the texture one pixel (or patch) at a time, while maintaining the spatial coherence with nearby pixels by

modeling the neighborhoods with Markov fields and fractal models [1, 2]. A weakness of these methods is that the spatial coherence between pixels is enforced at a local scale. A possible approach to circumvent this limitation consists of resorting to a small patch from which to grow the texture [3], or by using a multiscale setting [4, 5]. Global methods process the entire texture as a whole, using some criteria for measuring its similarity with a small texture patch. For example, the latter can be modeled with a statistical descriptor based on histograms [6] and Fourier coefficients [7].

Recently, an approach has been proposed in [8, 9], which introduces a preliminary step of dictionary learning for exploiting the given patch, and (not least) the Wasserstein distance for comparing the histograms of the entire texture with an extended version of the small patch. While the Wasserstein distance is well-known in image processing and computer vision under the name “earth mover distance” [10], it was only recently expanded to the context of texture synthesis [11, 9, 12].

Under the assumption that the main texture characteristics are contained in their Fourier magnitude [13], many works have shown that an efficient synthesis method is achieved when the texture phase is randomized [7, 9]. However, The resulting algorithm is limited to non-structured textures [14].

Regarding the problem considered in this paper, the authors in [15] propose to recover the high-resolution image from a pair of images: a complete low-resolution image and a high-resolution but incomplete one (sample). The resulting problem is solved using an extension of the nonlocal total variation model, where a set of connections is built between the missing high-resolution pixels and a set of pixels that lies in the sample. However, to interpolate the missing data, the authors in [16] design a new nonlocal graph that provides better connections between the missing pixels and the high-resolution pixels. Additionally, they introduce a histogram-based statistical prior modeled by a sum of Wasserstein distances between the histogram of some linear transformations of the texture.

The work in [17] exploits a patch-based nonlocal regularization and a Generalized Gaussian model of the texture gradients, whose parameters are learned on the high-resolution patch. Differently from [15] and [16], the authors in [17] use a prior

This study has been carried out with financial support from the French State, managed by the French National Research Agency (ANR) in the frame of the “Investments for the future” Programme IdEx Bordeaux - CPU (ANR-10-IDEX-03-02).

on the spatial covariance of the synthesized image.

In this paper, we propose a variational method that combines a histogram-based statistical prior [16] and a constraint on the power spectral density [17]. The main novelty of the proposed approach w.r.t. [16] lies in introducing a spectral constraint instead of the nonlocal regularization, and in considering the texture synthesis problem from free noise acquisitions with a high down-sampling factor. On the other hand, the originality of our technique w.r.t. [17] is twofolds: (i) the ability to consider multi-histogram priors without being constrained to a parametric model, (ii) the global optimization procedure that we carry out using a recent primal dual proximal algorithm.

The remainder of this paper is organized as follows. In Sec. 2, we present the texture synthesis as a nonconvex optimization problem. In Sec. 3, we propose to solve this problem by an iterative scheme based on proximal methods. Experimental results, showing the accuracy of the resulting images comparing with the state-of-the-art methods, are given in Sec. 4. Finally, some conclusions are drawn in Sec. 5.

1.2. Notations

Let $\|\cdot\|$ be the standard Euclidean norm, and let Id be the identity matrix. The domain of a function $f : \mathbb{R}^N \rightarrow]-\infty, +\infty]$ is $\text{dom } f = \{x \in \mathbb{R}^N | f(x) < +\infty\}$. $\Gamma_0(\mathbb{R}^N)$ is the class of lower semi-continuous convex functions from \mathbb{R}^N to $] -\infty, +\infty]$ such that $\text{dom } f \neq \emptyset$. Let $f \in \Gamma_0(\mathbb{R}^N)$. The conjugate of f is the function $f^* \in \Gamma_0(\mathbb{R}^N)$ defined by $f^* : \mathbb{R}^N \rightarrow]-\infty, +\infty] : u \mapsto \sup_{x \in \mathbb{R}^N} x^\top u - f(x)$. When f is Gâteaux-differentiable at $y \in \mathbb{R}^N$, $\partial f(y) = \{\nabla f(y)\}$ where $\nabla f(y)$ is the gradient of f at y . A differentiable convex function has β -Lipschitz continuous gradient ∇f if $(\forall (x, y) \in \mathbb{R}^N \times \mathbb{R}^N) \|\nabla f(x) - \nabla f(y)\| \leq \beta \|x - y\|$, where $\beta \in]0, +\infty[$. Let C be a nonempty subset of \mathbb{R}^N , then ι_C is the indicator function of C , equal to 0 on C and $+\infty$ otherwise.

2. PROPOSED APPROACH

Let $\bar{x} \in \mathbb{R}^N$ be the unknown signal to be recovered (which generally corresponds to an image of size $N = N_1 \times N_2$), $z^{(1)} \in \mathbb{R}^Q$ the complete low-resolution image, and $z^{(2)} \in \mathbb{R}^M$ the given sample¹ such that such that

$$z^{(1)} = D\bar{x}, \quad z^{(2)} = M\bar{x}, \quad (1)$$

where $D \in \mathbb{R}^{Q \times N}$ stands for spatial down-sampling by a dyadic factor in each direction yielding $Q = 2^{-r}N$, and $M \in \mathbb{R}^{M \times N}$ is a selection operator that extracts the patch from \bar{x} .

To recover \bar{x} from the observations $z^{(1)}$ and $z^{(2)}$, We propose a variational approach that leads to solving the following optimization problem:

$$\underset{x \in \mathbb{R}^N}{\text{minimize}} \quad \|Dx - z^{(1)}\|^2 + \iota_{C_1}(x) + H(x, z^{(2)}) + \iota_{C_2}(x), \quad (2)$$

¹A sample denotes a small patch of the synthesized image.

where $C_1 = \{x \in \mathbb{R}^N | Mx = z^{(2)}\}$. Beside the data fidelity terms w.r.t. the observations $z^{(1)}$ and $z^{(2)}$, we use two additional pieces of information: a term $H(\cdot, z^{(2)})$ conveying some histogram-based statistics, and a Fourier spectrum constraint C_2 . The histogram-based term is modeled through the Wasserstein distance discussed in Section 2.1, while the frequency constraint is presented in Section 2.2.

2.1. Statistical prior

The Wasserstein distance between the histograms² of two images $u \in \mathbb{R}^N$ and $v \in \mathbb{R}^N$ is defined as follows [11, 9]:

$$\mathcal{W}_2^2(\nu_u, \nu_v) = \min_{\sigma \in \Sigma_N} \|u - v \circ \sigma\|^2, \quad (3)$$

where ν_u and ν_v are the normalized histograms of u and v , the symbol $v \circ \sigma$ denotes a permutation of the vector v , and Σ_N is the set of all the permutations of N -length vectors. For grayscale images, the optimal permutation σ^* is computed as

$$\sigma^* = \sigma_v \circ \sigma_u^{-1}, \quad (4)$$

where σ_v (resp. σ_u) denotes the permutation operator that arranges the pixels of v (resp. u) in ascending order. In our case, however, the two images have a different number of pixels ($u \in \mathbb{R}^N$ and $v \in \mathbb{R}^M$, with $M < N$). Hence, we replicate the patch v so as to obtain a larger image $\tilde{v} \in \mathbb{R}^N$ such that the normalized histogram $\nu_{\tilde{v}}$ is equal to ν_v . Although the Wasserstein distance is nonconvex (due to the histogram transformation), its gradient is Lipschitz-continuous and takes the following form [8, 12]

$$\nabla_u \mathcal{W}_2^2(\nu_u, \nu_{\tilde{v}}) = 2(u - \tilde{v} \circ \sigma_{\tilde{v}} \circ \sigma_u^{-1}). \quad (5)$$

This property allows us to employ the Wasserstein distance into the optimization algorithm presented in Section 3.

In this work, inspired from [16], we define the term H in (2) as

$$H(x, z^{(2)}) = \sum_{s=1}^4 \alpha_s \mathcal{W}_2^2(\nu_{L_s x}, \nu_{z_s^{(2)}}) \quad (6)$$

where, for every $\forall s \in \{1, \dots, 4\}$, $\alpha_s > 0$, $z_s^{(2)} = L_s z^{(2)}$, $\tilde{z}_s^{(2)}$ is the extension of $z_s^{(2)}$ (after the linear transformation), and for every $s \in \{1, \dots, 4\}$, $L_s \in \mathbb{R}^{N_s \times N}$ is defined as follows

- L_1 : the identity matrix ($N_1 = N$).
- L_2 : the concatenation of the horizontal and vertical difference operators ($N_2 = 2N$).
- L_3 : the concatenation of the diagonal difference operators ($N_3 = 2N$).
- L_4 : the isotropic Laplacian operator ($N_4 = N$).

²The histogram of a signal refers to a histogram of the pixel intensity values.

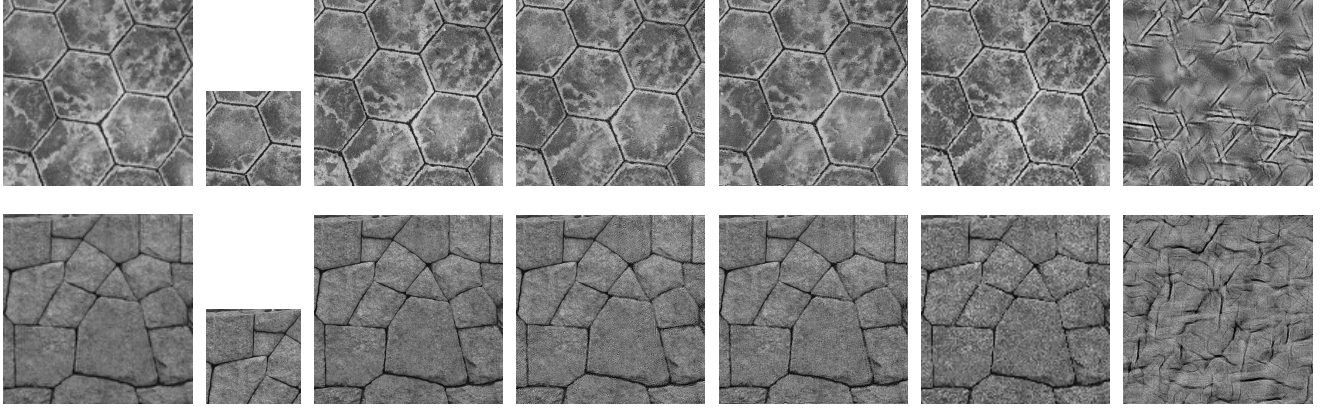


Fig. 1. From top to bottom: “Street”, “Wall”. From the left to the right: low-resolution image (which was up-sampled by a factor 4 for visualization purposes), high-resolution patch (25% of the total image), true image, the proposed approach without the spectral constraint, the proposed approach with the spectral constraint, the approach of [18] and the approach of [19].

2.2. Fourier Spectrum constraint

Textures having the same second-order statistics share a common auto-covariance and, therefore, a common Fourier magnitude. So it is meaningful to introduce a constraint enforcing texture characteristics while preserving the Fourier magnitude, through a random phase textures. Hence, inspired from [17], we search for an image $x \in \mathbb{R}^N$ such that

$$\forall m, |\hat{x}(m)| = |\hat{z}^{(2)}(m)|, \quad (7)$$

where \hat{x} (resp. $\hat{z}^{(2)}$) is the orthogonal discrete Fourier transform of x (resp. $z^{(2)}$), whose coefficients read

$$\hat{x}(m) = \frac{1}{N_1 N_2} \sum_{p \in \mathbb{R}^N} x(p) e^{-2i\pi(\frac{p_1 p_1}{N_1} + \frac{p_2 p_2}{N_2})}. \quad (8)$$

Consequently, Eq. (7) can be rewritten as a Fourier spectrum constraint defined as

$$C_2 = \{x \in \mathbb{R}^N \mid \forall m, \exists \varphi(m) : \hat{x}(m) = e^{i\varphi(m)} \hat{z}^{(2)}(m)\} \quad (9)$$

Since x and $z^{(2)}$ are real images, $\varphi(m)$ of Eq. (9) must be antisymmetric modulo 2π . The projection onto the convex set C_2 consists in putting together the phase and the modulus, whose expression is given in Sec. 3.

Discussion We observed that Gaussian textures could be accurately synthesized using the spectral constraint introduced in Eq. (9). However, for structural textures with important oscillations, the latter hypothesis is not valid. Nonetheless, taking into account the statistical information through histogram priors and the low frequencies provided by the low-resolution acquisition, the proposed approach (see Eq. (2)) infers the correct structures and details of the sample to the estimated texture, leading to improved results w.r.t. the classical spectral prior considered alone.

3. OPTIMIZATION

The solution of Eq. (2) requires an efficient algorithm for dealing with problems involving nonsmooth functions and linear operators. Recently, it has been shown experimentally that primal-dual proximal methods [20, 21, 22, 23, 24, 25], which were originally designed for convex optimization, can be also applied to nonconvex problems in some circumstances [26, 27]. In the convex setting, the key tool of these methods is the proximity operator [28] of a lower semicontinuous convex function $f: \mathbb{R}^N \mapsto -\infty; +\infty$, defined as

$$(\forall y \in \mathbb{R}^N) \quad \text{prox}_f(y) = \underset{z \in \mathbb{R}^N}{\text{argmin}} \quad f(z) + \frac{1}{2} \|z - y\|^2.$$

Proximity operators enjoy many properties [29]. In particular, they generalize the notion of projection onto a closed convex set C , in the sense that $\text{prox}_{\iota_C} = P_C$. Among the wide array of existing proximal algorithms, we employ the Forward-Backward Primal Dual method (FBPD) [24] reported in Algorithm 1.

Algorithm 1 FBPD [24]

INITIALIZATION

$$\left[\begin{array}{l} \text{Choose } (x^{[0]}, y^{[0]}) \in \mathbb{R}^n \times \mathbb{R}^{K^n} \\ \text{set } \tau > 0 \text{ and } \omega > 0 \text{ such that } \tau(\beta/2 + \omega) < 1 \end{array} \right.$$

FOR $l = 0, 1, \dots$

$$\left[\begin{array}{l} \hat{x}^{[l]} = \nabla f(x^{[l]}) + y^{[l]} \\ x^{[l+1]} = P_{\{M \cdot = z^{(2)}\}}(x^{[l]} - \tau \hat{x}^{[l]}) \\ \hat{y}^{[l]} = (2x^{[l+1]} - x^{[l]}) \\ y^{[l+1]} = y^{[l]} + \omega \hat{y}^{[l]} - P_{C_2}(y^{[l]} + \omega \hat{y}^{[l]}) \end{array} \right.$$

The operators required by this algorithm are detailed below.

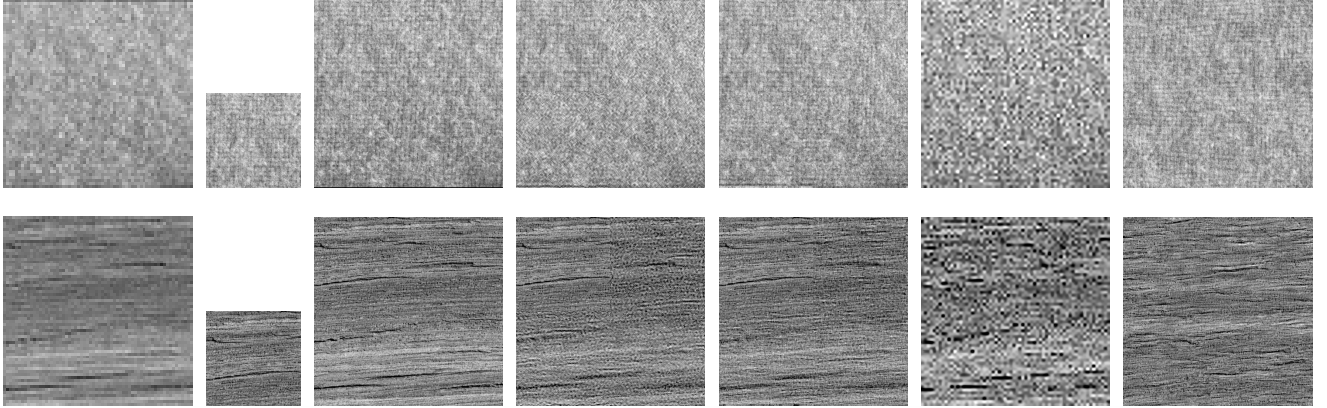


Fig. 2. From top to bottom: “Woolen”, “Wood”. From the left to the right: low-resolution image (which was up-sampled by a factor 8 for visualization purposes), high-resolution patch (25% of the total image), true image, the proposed approach without the spectral constraint, the proposed approach with the spectral constraint, the approach of [18] and the approach of [19].

- The projection onto the set C_2 is given by the following expression

$$P_{C_2}(\hat{x}(m)) = \frac{\hat{x}(m) \cdot \hat{z}^{(2)}(m)}{|\hat{x}(m) \cdot \hat{z}^{(2)}(m)|} \hat{z}^{(2)}(m), \quad (10)$$

where $x \cdot y$ denotes the hermitian product.

- The projection onto the convex set associated to the constraint $Mx = z^{(2)}$ is expressed as

$$P_{\{M=z^{(2)}\}}(x) = x + M^\top (z^{(2)} - Mx). \quad (11)$$

- The gradient of the sum of the remaining terms, that is $f(x) = \|Dx - z^{(1)}\|^2 + \sum_{s=1}^4 \alpha_s \mathcal{W}_2^2(\nu_{L_s x}, \nu_{z_s^{(2)}})$, reads

$$\begin{aligned} \nabla f &= 2D^\top (Dx - z^{(1)}) \\ &+ 2 \sum_{s=1}^4 \alpha_s L_s^\top (L_s x - \tilde{z}_s^{(2)} \circ \sigma_{z_s^{(2)}} \circ \sigma_{L_s x}^{-1}), \end{aligned} \quad (12)$$

where ∇f is β -Lipschitz with $\beta = 2(1 + \sum_1^4 \alpha_s \|L_s\|^2)$.

Although there is no theoretical guarantee about the estimate produced by Algorithm 1, in our experiments we observed that it always converges to a stable solution.

4. EXPERIMENTAL RESULTS

4.1. Algorithm and Initialization

We address the problem by considering a hierarchical approach, which consists of initializing our algorithm with the low-resolution image and iterating three consecutive steps: (i) up-sample the initialization by a factor 2 using a bicubic interpolation, (ii) apply a patch-based approach [30], and (iii) run the FBPD algorithm. These three steps are repeated in loop until the size of the output signal is equal to the sought one (512x512 in our case).

4.2. Results

This section provides numerical results of our synthesis algorithm. We illustrate the effect of the Fourier constraint on the outcome of Eq. (2). We compare our results to the most classical synthesis method [31] and to that of super-resolution method [18]. Fig. 1 gives two texture examples where the down-sampling factor is equal to 4, and the sample amounts to 25% of the total image. As illustrated by these experiments, we assess the performance achieved with and without the spectral constraint. Using the proposed formulation (2), we obtain the best visual results while the state-of-the-art super-resolution method [18] tends to smooth the textures and the state-of-the-art texture synthesis approaches [19] produce an image (by replicating the patch) without exploiting information provided by the low-resolution image. Hence, the results may be far from the ground truth. Fig. 2 gives a similar example where the down-sampling factor is equal to 8 and the sample amounts to 25% of the total image. The obtained results are better than the ones achieved without the spectral prior. Formulation (2) leads to a better texture reconstruction in the synthesized images compared to the state-of-the-art methods. This is confirmed by looking at the reconstructed textures and the low-resolution image. Even if the synthesized image of [19] is close to the sample but it is far from the low-resolution guide.

5. CONCLUSIONS AND FUTURE WORK

In this paper, we have investigated the application of texture synthesis guided by a low resolution image. The proposed approach is adequate for various texture images. It is also able to exploit the potentials offered by multicore/GPU parallel architectures. However, one of the current limitations of the proposed method is that it is nonconvex, thus requiring a good initialization. In our future work, we therefore plan to consider a convex relaxation of the histogram prior in order to have a convex minimization problem [32].

6. REFERENCES

- [1] G. Cross and A. Jain, "Markov random field texture models," *IEEE Trans. Pattern Anal. Mach. Int.*, no. 1, pp. 25–39, Jan. 1983.
- [2] V. Kwatra, I. Essa, A. Bobick, and N. Kwatra, "Texture optimization for example-based synthesis," *ACM Trans. Graph.*, vol. 24, no. 3, pp. 795–802, 2005.
- [3] S. Lefebvre and S. Hoppe, "Parallel controllable texture synthesis," *Trans. on graphics*, vol. 24, no. 3, pp. 777–786, 2005.
- [4] C. Han, E. Risser, R. Ramamoorthi, and E. Grinspun, "Multi-scale texture synthesis," *ACM Trans. Graph.*, vol. 27, no. 3, pp. 51:1–51:8, 2008.
- [5] M. Eisemann and M. Magnor, "ZIPMAPS: zoom-into-parts texture maps," in *Proc. Vision Modeling and Visualization*, Siegen, Germany, 2010, pp. 291–297.
- [6] D. Heeger and J. Bergen, "Pyramid-based texture analysis/synthesis," in *Conf. on Comput. Graphics and Interactive Tech.*, Washington, USA, 1995, pp. 229–238.
- [7] B. Galerne, Y. Gousseau, and J.-M. Morel, "Random phase textures: Theory and synthesis," *Image Process On Line*, vol. 1, 2011.
- [8] G. Tartavel, Y. Gousseau, and G. Peyré, "Constrained sparse texture synthesis," in *Scale Space and Variational Methods in Computer Vision*, Arjan Kuijper, Kristian Bredies, Thomas Pock, and Horst Bischof, Eds., vol. 7893 of *Lecture Notes in Computer Science*, pp. 186–197. Springer Berlin Heidelberg, 2013.
- [9] G. Tartavel, Y. Gousseau, and G. Peyré, "Variational texture synthesis with sparsity and spectrum constraints," *J. Math. Imaging Vision*, vol. 52, no. 1, pp. 124–144, May 2015.
- [10] Y. Rubner, C. Tomasi, and L. J. Guibas, "The earth mover's distance as a metric for image retrieval," *Int. J. Comput. Vision*, vol. 40, no. 2, pp. 99–121, Nov. 2000.
- [11] J. Rabin and G. Peyré, "Wasserstein regularization of imaging problem," in *Proc. IEEE Int. Conf. Image Process.*, Brussels, Belgium, Sep. 2011, pp. 1541–1544.
- [12] G. Tartavel, G. Peyré, and Y. Gousseau, "Wasserstein loss for image synthesis and restoration," 2016, HAL-1292843.
- [13] B. Julesz, "Visual pattern discrimination," *IEEE Trans. Inf. Theory*, vol. 8, no. 2, pp. 84–92, Feb. 1962.
- [14] A. Desolneux, L. Moisan, and S. Ronsin, "A compact representation of random phase and gaussian textures," in *Proc. IEEE Int. Conf. Acoust., Speech Signal Process.*, Kyoto, Japan, Mar. 2012, pp. 1381–1384.
- [15] M. Hidane, M. El Gheche, J.-F. Aujol, Y. Berthoumieu, and C.-A. Deledalle, "Image zoom completion," 2015, HAL-01253124.
- [16] M. El Gheche, J.-F. Aujol, Y. Berthoumieu, and C.-A. Deledalle, "Texture reconstruction guided by the histogram of a high-resolution patch," 2016, HAL-01276582.
- [17] R. Fablet and F. Rousseau, "Joint interpolation of multi-sensor sea surface temperature fields using non-local and statistical priors," 2016, HAL-01216762.
- [18] W. Dong, L. Zhang, G. Shi, and X. Wu, "Image deblurring and super-resolution by adaptive sparse domain selection and adaptive regularization," *IEEE Trans. Image Process.*, vol. 20, no. 7, pp. 1838–1857, Jul. 2011.
- [19] J. Portilla and E. P. Simoncelli, "A parametric texture model based on joint statistics of complex wavelet coefficients," *Int. J. Comput. Vision*, vol. 40, no. 1, pp. 49–71, Oct. 2000.
- [20] A. Chambolle and T. Pock, "A first-order primal-dual algorithm for convex problems with applications to imaging," *J. Math. Imaging Vision*, vol. 40, no. 1, pp. 120–145, May 2011.
- [21] L. M. Briceño-Arias and P. L. Combettes, "A monotone + skew splitting model for composite monotone inclusions in duality," *SIAM J. Optim.*, vol. 21, no. 4, pp. 1230–1250, Oct. 2011.
- [22] P. L. Combettes and J.-C. Pesquet, "Primal-dual splitting algorithm for solving inclusions with mixtures of composite, lipschitzian, and parallel-sum type monotone operators," *Set-Valued Var. Anal.*, vol. 20, pp. 2, Jun. 2012, 22 pp.
- [23] B. C. Vũ, "A splitting algorithm for dual monotone inclusions involving cocoercive operators," *Adv. Comput. Math*, vol. 38, no. 3, pp. 667–681, Apr. 2013.
- [24] Laurent Condat, "A primal-dual splitting method for convex optimization involving lipschitzian, proximable and linear composite terms," *J. of Optim. Theory and Appl.*, vol. 158, no. 2, pp. 460–479, Aug. 2013.
- [25] N. Komodakis and J.-C. Pesquet, "Playing with duality: An overview of recent primal-dual approaches for solving large-scale optimization problems," *IEEE Signal Processing Magazine*, vol. 6, no. 32, pp. 31–54, Nov. 2015.
- [26] M. Storath, A. Weinmann, and L. Demaret, "Jump-sparse and sparse recovery using Potts functionals," *IEEE Trans. on Signal Process.*, vol. 62, no. 14, pp. 3654–3666, Jul. 2014.
- [27] T. Möllenhoff, E. Strelakowskiy, M. Moeller, and D. Cremers, *Energy Minimization Methods in Computer Vision and Pattern Recognition: 10th International Conference, EMMCVPR 2015, Hong Kong, China, Jan. 13-16, 2015. Proceedings*, chapter Low Rank Priors for Color Image Regularization, pp. 126–140, Springer International Publishing, Cham, 2015.
- [28] J. J. Moreau, "Fonctions convexes duales et points proximaux dans un espace hilbertien," *C. R. Acad. Sci.*, vol. 255, pp. 2897–2899, 1962.
- [29] P. L. Combettes and J.-C. Pesquet, "Proximal splitting methods in signal processing," in *Fixed-Point Algorithms for Inverse Problems in Science and Engineering*, H. H. Bauschke, R. Burachik, P. L. Combettes, V. Elser, D. R. Luke, and H. Wolkowicz, Eds., pp. 185–212. Springer-Verlag, New York, USA, 2011.
- [30] A. Efros and W. Freeman, "Image quilting for texture synthesis and transfer," *Computer Graphics Proceedings, Annual Conference Series*, pp. 341–346. ACM Press / ACM SIGGRAPH, Aug. 2001.
- [31] J. Portilla and E. P. Simoncelli, "A parametric texture model based on joint statistics of complex wavelet coefficients," *Int. J. Comput. Vision*, no. 1, pp. 49–70, 2000.
- [32] P. Swoboda and C. Schnörr, "Convex variational image restoration with histogram priors," *SIAM J. Imaging Sciences*, vol. 6, no. 3, pp. 1719–1735, 2013.